Published in final edited form as:
Ultrasound Med Biol. 2009 October ; 35(10): 1709–1721. doi:10.1016/j.ultrasmedbio.2009.04.019.

In-Vivo Quantification of Liver Stiffness in a Rat Model of Hepatic Fibrosis with Acoustic Radiation Force

Michael H Wang[a], **Mark L Palmeri**[a], **Cynthia D Guy**[c], **Liu Yang**[d], **Laurence W Hedlund**[b], **Anna Mae Diehl**[d], and **Kathryn R Nightingale**[a]

[a] Department of Biomedical Engineering, Duke University

[b] Center for In Vivo Microscopy, Duke University Medical Center

[c] Department of Pathology, Duke University Medical Center

[d] Division of Gastroenterology, Duke University Medical Center

Abstract

Liver fibrosis is currently staged using needle biopsy, a highly invasive procedure with a number of disadvantages. Measurement of liver stiffness changes that accompany progression of the disease may provide a quantitative and non-invasive method to assess the health of the liver. The purpose of this study is to investigate the correlation between liver stiffness measured by radiation force induced shear waves and disease related changes in the liver. An additional aim is to present initial findings on the effects of liver viscosity on radiation force induced shear wave morphology. Liver fibrosis was induced in 10 rats using carbon tetrachloride (CCl_4), while 5 rats acted as controls. Liver stiffness was measured *in vivo* in all rats after a treatment period of 8 weeks using a modified Siemens SONOLINE Antares™ scanner. The spatial coherence of radiation force induced shear waves propagating in the viscoelastic rat liver decreased significantly with propagation distance, compared to shear waves in an elastic phantom, and a finite element model of a purely elastic medium. Animals were sacrificed after imaging and liver samples were taken for histopathological analysis and collagen quantification using picosirius red staining and hydroxyproline assay. At the end of the treatment period, 5 rats had healthy livers (stage F0), while 6 had severe fibrosis (F3), and the rest had light to moderate fibrosis (F1 and F2). The measured liver stiffness for the F0 group was 1.5 ± 0.1*kPa* (mean ± 95% confidence interval), and for F3 livers was 1.8 ± 0.2*kPa*. In this study, liver stiffness was found to be linearly correlated with the amount of collagen in the liver measured by picosirius red staining ($r^2 = 0.43$, $p = 0.008$). In addition, stiffness spatial heterogeneity was also linearly correlated with liver collagen content ($r^2 = 0.58$, $p = 0.001$) by picosirius red staining. These results are consistent with those obtained by Salameh et al (2007) and Yin et al (2007b) using animal models of liver fibrosis and MR elastography. This suggests that stiffness measurement using acoustic radiation force can provide a quantitative assessment of the extent of fibrosis in the liver and can be potentially used for the diagnosis, management, and study of liver fibrosis.

Keywords

acoustic radiation force; hepatic fibrosis; CCl_4 rat model; shear wave; stiffness; ultrasound

Corresponding Author: Michael Wang, Addr: Room 136 Hudson Hall, Box 90281, Durham, NC 27708-0281, Email: michael.h.wang@duke.edu, Ph: (919) 660-5525.

Introduction

Liver fibrosis is the common result of various causes of chronic damage to the liver, including infections, toxins, autoimmune disorder, cholestatic and metabolic diseases (Friedman, 2003). Fibrosis is marked by the gradual replacement of hepatocytes by extracellular collagen, which disturbs the normal architecture of the liver and can inhibit its ability to function. Cirrhosis, the end stage of fibrosis, affects millions of people worldwide. In the US, an estimated 900,000 patients suffer from cirrhosis, resulting in 30,000 deaths per year (Friedman, 2003).

Liver biopsy is the current gold standard for the diagnosis of liver fibrosis. However, this procedure has numerous disadvantages. It is highly invasive and is associated with potential morbidity and mortality (Piccinino et al, 1986). It can also be prone to sampling error, particularly when small biopsy samples are analyzed (Ratziu et al, 2005). In addition, inter-observer variability of up to 20% in assessing the degree of fibrosis is possible (Friedman, 2003). Lastly, repeat liver biopsies are not well tolerated, and therefore not appropriate for monitoring disease progression or response to antifibrotic therapies. Therefore, there is an immediate need for an non-invasive, low cost, and outpatient-friendly method for the assessment of liver fibrosis.

Recently, there has been increasing interest in the measurement of liver stiffness as a marker for hepatic fibrosis. This is based on the observation that liver stiffness increases with the progression of fibrosis (Yeh et al, 2002). Several imaging-based techniques for the non-invasive measurement of liver stiffness have been developed. The Fibroscan® system (Echosens, Paris, France) (Sandrin et al, 2003) uses a piston-like vibrator to punch the body wall in order to induce shear waves inside the liver. A single-element ultrasound transducer at the end of the vibrator is able to measure the resulting tissue displacement as a function of time, from which the shear wave velocity, and liver stiffness is derived. Clinical trials of the Fibroscan® have shown its stiffness measurements to be significantly correlated with fibrosis stage (Takeda et al, 2006; Carrión et al, 2006; Castéra et al, 2005). Magnetic resonance elastography (MRE) is another promising method for non-invasive *in vivo* measurement of liver stiffness. In prospective studies of MRE in patients (Huwart et al, 2006; Yin et al, 2007a), low frequency shear waves (~ 60 *Hz*) were generated in the liver using an external piston coupled to the body wall. These shear waves were monitored by specialized MRE pulse sequences, and images of tissue stiffness were reconstructed using local inversion algorithms. Both Huwart et al (2006) and Yin et al (2007a) reported increasing liver stiffness measured by MRE with fibrosis stage assessed by liver biopsy. These two groups have also explored the use of MRE in controlled animal models of liver fibrosis (Salameh et al, 2007; Yin et al, 2007b). Both of these studies showed significant correlations between measured stiffness and quantitative measures of fibrosis.

Acoustic radiation force generated by ultrasound can also be used to interrogate the mechanical properties of tissue *in vivo* and non-invasively. In contrast to systems which use external mechanical vibrators to excite deeper tissue of interest, acoustic radiation force provides mechanical excitation directly to the focal region of the acoustic beam (Nyborg, 1965). Therefore, mechanical energy can be delivered by acoustic radiation force to deep-lying tissue (+8cm using a diagnostic ultrasound scanner) (Fahey et al, 2005) even in the presence of intervening fat layers or ascites, which limits utility of the Fibroscan® system (Foucher et al, 2006). An additional limitation of the Fibroscan® is the small volume of liver tissue sampled (a cylinder approximately 2*cm* long and 2*cm* in diameter). Although the volume of tissue interrogated around each focal zone of acoustic radiation force excitation is also small

(typically a cylinder approximately 2*cm* long and 1*cm* in diameter), multiple excitations can be used to sample a larger volume of tissue.

Several approaches for measuring tissue stiffness by monitoring its dynamic response to acoustic radiation force using ultrasound imaging have been proposed. These include shear wave elasticity imaging (SWEI) (Sarvazyan et al, 1998), supersonic shear imaging (SSI) (Bercoff et al, 2004), shear wave dispersion ultrasound vibrometry (SDUV) (Chen et al, 2004), localized harmonic motion imaging (Konofagou and Hynynen, 2003), spatially modulated radiation force (SMURF) (McAleavey et al, 2007), and acoustic radiation force impulse imaging (ARFI) (Nightingale et al, 2002). In addition to ultrasound, magnetic resonance monitoring of shear waves generated by acoustic radiation force is also possible (McDannold and Maier, 2008), and could allow MRE to be performed in the body where external mechanical excitation is not feasible.

In addition to liver stiffness, the relationship between its viscoelastic (VE) properties and fibrosis have also been explored (Salameh et al, 2007; Huwart et al, 2006). Viscoelasticity is a material property in which the shear wave speed is frequency dependent (dispersive). By modeling liver as a Voigt solid, Huwart et al (2006) was able to reconstruct images of liver shear viscosity from MRE data. The mean shear viscosity of livers with cirrhosis was found to be significantly higher than healthy livers, suggesting that shear viscosity could also be useful for the assessment of liver fibrosis. Salameh et al (2007) used the same imaging approach on rats, and found significant correlations between viscosity and the amount of fibrosis in the liver. Imaging of tissue viscoelastic parameters with acoustic radiation force techniques, including SDUV (Chen et al, 2004) and SSI (Tanter et al, 2008), have also been investigated for its potential in detecting pathological changes in various types of tissue.

A technique using acoustic radiation for the quantification of tissue stiffness has recently been described by Palmeri et al (2008). A similar approach to that originally proposed by Sarvazyan et al (1998) and SSI (Bercoff et al, 2004) is taken, in which shear waves are induced in tissue by focused impulsive acoustic radiation force and their propagation speed is monitored by ultrasound to quantify tissue shear modulus. This method uses the same diagnostic transducer for excitation and tracking of shear wave displacement, and can therefore be implemented on a diagnostic ultrasound scanner without additional hardware. In contrast to Fibroscan®, this approach allows image guidance of the exact excitation location, enabling verification that stiffness measurements were performed in the intended organ. Finally, compared to MRE, which can require acquisition times of up to 20 minutes (Huwart et al, 2006), stiffness measurements using ultrasound imaging can be performed within seconds, facilitating its use in a clinical environment.

The purpose of this study is to evaluate the feasibility of using acoustic radiation force and processing methods as proposed by Palmeri et al (2008) to detect stiffness changes in rat livers caused by chemically induced fibrosis, and compare measured liver stiffness with histopathological evaluation of the disease stage, as well as quantitative measurements of fibrosis in the liver using picosirius red staining and hydroxyproline assay. A secondary goal is to present initial investigations of quantifying the effects of viscoelasticity on shear waves propagating in the normal and diseased rat livers.

Background

Acoustic radiation force arises from the transfer of momentum from a propagating acoustic wave in a lossy medium by absorption or reflection. The spatial distribution of the resulting force field is dependent on both the excitation beam geometries and acoustic properties of the

medium. For soft tissues, where the major contribution to attenuation is due to absorption, the radiation force magnitude under plane wave assumptions is given by (Nyborg, 1965)

$$F=\frac{W_{absorbed}}{c}=\frac{2\alpha I}{c}, \tag{1}$$

where F is the acoustic radiation force in the direction of the propagating wave, $W_{absorbed}$ is the power absorbed by the medium at a given spatial location, c is the speed of sound in the medium, α is the absorption coefficient of the medium, and I is the temporal average intensity at a given location. The force field (or region of excitation) always lies within the geometric shadow of the active transmit aperture and is typically most energetic near the focal point.

In addition to radiation force, acoustic energy absorbed by a lossy medium is also converted to heat. In tissue, the rate of heat generation per unit volume q_v for a progressive plane wave is given by (Nyborg, 1981)

$$q_v=2\alpha I. \tag{2}$$

The maximum temperature increase ΔT, assuming no heat loss by convection or conduction, can be approximated by (Fry and Fry, 1953)

$$\Delta T=\frac{q_v}{c_v}t=\frac{2\alpha I}{c_v}t, \tag{3}$$

where c_v is the heat capacity per unit volume of soft tissue, and t is the exposure time.

In this study, acoustic radiation force in tissue is generated by a short duration focused ultrasound pulse (see Table 1 for parameters). This force generates maximum displacement amplitudes of typically 20μm at the focus inside the rat liver. The radiation force from the excitation pulse induces shear oscillations which propagate away from the region of excitation. As will be detailed later, by monitoring the tissue motion near the region of excitation spatially and temporally using 1D speckle tracking methods, the shear wave speed inside the rat liver can be estimated. The shear wave velocity (c_T) can then be related to the shear modulus (G) and density (ρ) under assumptions of a linear elastic isotropic material by

$$G=\rho c_T^{\,2}. \tag{4}$$

Methods

Animal Model

Studies were performed on 5 week old male Sprague-Dawley rats weighing 120–140g using procedures approved by the Duke University IACUC. Liver fibrosis was induced by intraperitoneal (i.p.) injections of 1.0ml/kg body weight of 10% carbon tetrachloride (CCl_4) (Fisher Scientific, Pittsburgh, PA, USA) in olive oil (Fisher Scientific, Pittsburgh, PA, USA), three times a week for eight weeks. CCl_4 is one of the oldest and most widely used toxins for the induction of liver fibrosis in animals. Its pattern of pathogenesis resembles some aspects

of alcoholic liver damage in humans (Tsukamoto et al, 1990). A treatment group of 10 animals were given the CCl_4, while 5 control animals were injected with the same dose of olive oil only. Injections were stopped and imaging was performed after eight weeks, at which time moderately severe fibrosis (stage F2–F3) was produced by the model.

Data Acquisition

A modified Siemens SONOLINE Antares™ scanner (Siemens Medical Solutions USA, Ultrasound Division, Issaquah, WA, USA) was used for radiation force measurement of liver stiffness. Acquisition parameters are summarized on Table 1. The acquisition sequence consists of a reference track A-line, followed by a high intensity pushing line to mechanically excite the tissue, then by repeated tracking A-lines in the same location as the reference to monitor tissue motion.

Eighty tracking A-lines were used at a pulse repetition frequency (PRF) of 9.4*kHz*, providing 8.5*ms* of data at each tracking location. To monitor the shear wave propagation away from the excitation location, a series of tracking locations laterally offset to one side of the push were used. 4:1 parallel receive was implemented to reduce the number of interrogations required. A total of nine repeated excitations in the same location with tracking locations increasingly further away laterally for each excitation were used to measure shear wave propagation in a lateral region of approximately 5*mm*. This sequence was repeated in five different push locations within each imaging plane, separated by 2.5*mm* laterally. The combined lateral region of interest (ROI) interrogated by the five pushes (measured from the location of the first push to the edge of the tracking window of the last push) was approximately 16*mm*.

To estimate tissue heating associated with the acquisition sequence, hydrophone measurements (Model 805, Sonic Technologies, Hatboro, PA) of the peak acoustic intensity output of the pushing pulse was made. Hydrophone measurements were conducted at the excitation focal depth of 25*mm* in a 60% by volume evaporated milk solution, which simulated the acoustic attenuation of rat liver. A 15*mm* water-path between the transducer and milk solution separated by saran wrap was used to replicate the water-path used to couple the transducer to the rat abdomen during imaging. The spatial peak pulse average intensity (I_{sppa}) was measured for ten cycles of the pushing pulse with parameters shown in Table 1. The recorded peak pressure is shown in Figure 1. Only ten cycles were used for focal measurements to avoid damage to the hydrophone. Power supply droop for the full 200 cycle pushing pulse was measured with the hydrophone in the near-field of the transducer, and a correction term for the I_{sppa} measured over ten cycles was used. Finally, a derating term accounting for the acoustic attenuation of the rat abdominal wall, assumed to be 1.1*dB*/*cm*/*MHz* (Teotico et al, 2001) and 5mm in thickness, and for the difference in the measured acoustic attenuation of the evaporated milk solution (0.3*dB*/*cm*/*MHz*) and that of rat liver (assumed to be 0.5*dB*/*cm*/*MHz*), was included to arrive at an estimate of $3054 W/cm^2$ for the *in situ* I_{sppa}. This value, along with a heat capacity per unit volume of $c_v = 4200 mW{\cdot}s/cm^3/°C$, an exposure time of $t = 61\mu s$, and Equation (3), was used to estimate a peak temperature rise of $\Delta T = 0.02°C$ during a single push. The time between repeated push pulses in the same location is 8.3*ms*. Assuming that negligible cooling occurs in this time, the total cumulative peak temperature rise due to the nine repeated pushes of the acquisition sequence is estimated to be 0.18°C.

Liver stiffness was measured in all animals 3–5 days after the last injection. During imaging, the rats were anesthetized with isoflurane and placed supine on a warming platform (Vevo Mouse Handling Table, Visualsonics, Toronto, ON, Canada). The ultrasound probe was coupled to the rat through a water-path and a thin layer of saran wrap holding the water. The water level above the rat was kept constant for all the animals and the water-path from the abdomen to the transducer face was typically around 15*mm*. Abdominal hair was removed before coupling and a thin layer of gel was placed between the saran wrap and skin surface.

Respiration was monitored by a capacitive sensor on the warming platform. The resulting signal was connected to the Physio Module of the Antares™ as described by Ashfaq et al (2005) to trigger data acquisition in order to minimize the effect of respiratory motion on tissue displacement. Typically, stiffness measurements were performed at 10–30 sagittal planes separated by 1*mm* through the entire visible area of the rat liver. A rail system connected to the transducer holder was used to move the probe between imaging planes (Vevo Integrated Rail System, Visualsonics, Toronto, ON, Canada).

Animals were sacrificed immediately after stiffness measurements by cardiac injection of pentobarbital. Livers were harvested, weighed, and fixed in 10% buffered formalin for histopathological analysis. Slides were made from 5 micron thick slices of the right and left lobes and stained with Masson's trichrome. Additional slides of the rat livers were stained with picosirius red (Sigma-Aldrich, St. Louis, MO, USA) for collagen and counterstained with fast green (Sigma-Aldrich, St. Louis, MO, USA). Small pieces (26–144*mg*) of liver tissue from the left lobe were freeze-dried for hydroxyproline analysis.

Data Processing

Tissue motion due to acoustic radiation force excitation was measured by Loupas' method on IQ data (Pinton et al, 2006) and subsequently using a dynamic motion filter to reduce physiological motion artifacts (Palmeri et al, 2008). Displacement data was averaged over 0.5*mm* sliding windows ±1*mm* around the focal depth in the axial dimension to reduce noise. In addition, a low-pass filter with a cutoff frequency of 1*kHz* was used to remove high frequency jitter. The tissue displacement at the focal depth lateral to the excitation location obtained *in vivo* in one rat liver is displayed in Figure 2. The curves in the figure correspond to the axial displacement at the focal depth at different lateral tracking locations as a function of time after the excitation pulse. Shear wave propagation and attenuation of its amplitude away from the push location can be readily observed.

Shear moduli were reconstructed from displacement data using the lateral time-to-peak (TTP) algorithm (Palmeri et al, 2008). This time-of-flight algorithm measures the velocity of the shear wave by finding its peak displacement time at lateral locations away from the excitation region. The shear wave speed is then estimated at each depth by performing a linear regression of the TTP data versus lateral location, assuming purely lateral shear wave propagation and that the peak displacement propagates at the shear wave speed. Regressions were performed over a lateral window sized such that the maximum displacement occurring over time was greater than 1μm at every lateral position. In addition, data within the excitation beamwidth laterally (typically 1mm) was not used for the regression. Finally, Equation (4), along with an assumed tissue mass density of $\rho = 1 g/cm^3$, was used to convert shear wave speed to shear modulus.

To evaluate the effect of viscosity on shear wave morphology in the rat livers, its spatial coherence function was calculated at the excitation focal depth for a range of distances lateral to the excitation. Raw displacement data ±1*mm* around the focal depth axially was averaged and low-pass filtered as previously, but no motion filtering was performed in order to preserve the shape of the waveforms. The spatial coherence was calculated as the maximum of the cross-correlation function of the shear wave at a location of interest, and a reference location. The reference, representing the 'initial' shape of the shear wave, was chosen as the lateral location closest to the radiation force excitation having a displacement at the first time-point below 2μm. This was done to ensure that the front edge of the shear wave at the reference location was not distorted by excessive reverb from the excitation pulse. As for shear wave speed estimation, data within the excitation beamwidth laterally, where significant diffraction of the shear wave occurs, was not used. Finally, by varying the location of interest from the reference to locations farther from the excitation, the shear wave spatial coherence was found as a function of propagation distance.

As the propagation distance increases, changes to the shear wave morphology due to dispersion are expected to become more significant, and its spatial coherence will decrease as a result. Therefore, in dispersive media, the shear wave spatial coherence should decrease with propagation distance. In non-dispersive media, changes in spatial coherence with distance should be negligible. As a measure of change in shear wave morphology in the rat liver, a line was fit using the method of least squares to the spatial coherence as a function of propagation distance. Fits with a coefficient of determination less than 0.8 and a 95% confidence interval (CI) more than 0.003 were discarded. The magnitude of the slope of this line was used for characterizing changes in shear wave morphology, and will be referred to as the decorrelation rate.

As a baseline for comparison, a simulation of the dynamic response of a purely elastic medium to acoustic radiation force excitation was performed using the finite element method (FEM) (Palmeri et al, 2005). The simulated excitation beam configuration was the same as that used for *in vivo* imaging, as outlined in Table 1. In addition, ten acquisitions using the same imaging sequence employed for the rats were obtained in different locations of a homogeneous and elastic phantom (CIRS, Norfolk, VA, USA). The shear wave decorrelation rate in both the simulation and phantom data were measured as described above, and were expected to be small due to the lack of viscosity.

Pathology slides stained with Masson's trichrome were examined by a pathologist (C.D.G.) and the severity of fibrosis in each rat was staged using the modified Brunt score (Kleiner et al, 2005) from F0 (no fibrosis) to F4 (cirrhosis). Steatosis, lobular inflammation, and hepatocyte ballooning, are other features associated with chronic liver disease. Steatosis and inflammation, in particular, have been explored as potential factors influencing liver stiffness (Yin et al, 2007a; Arena et al, 2008). Therefore, Steatosis (S0 - S3), inflammation (L0 - L3), and hepatocyte ballooning (B0 - B2) were evaluated along with fibrosis by the same pathologist, and a combined score (NAS0 - NAS8) for nonalcoholic steatohepatitis (NASH) was given (Kleiner et al, 2005). Slides stained with picosirius red were examined under a microscope at 10× magnification and 10 random fields ($0.90 \times 0.67 mm$) from each slide were chosen for collagen quantification. The total area containing collagen was determined by color thresholding using MetaMorph software (Molecular Devices, Sunnyvale, CA, USA), and this was expressed as a percentage of the total area of the 10 samples. Hydroxyproline content was measured from the freeze-dried liver specimens using procedures previously described by Yamaguchi et al (2007).

Statistical Analysis

Shear wave speed regressions with a coefficient of determination more than 0.8 and a 95% confidence interval (CI) less than 0.2 were kept as valid estimates for modulus reconstruction. A single stiffness value for each location interrogated with radiation force was obtained by averaging the modulus reconstructions within $\pm 1 mm$ of the excitation focal depth, corresponding to 5 axial samples. Locations with less than 3 valid modulus reconstructions within this range were discarded. Depths close to the focus were chosen to reduce possible errors from non-lateral propagation of the shear wave at depths farther from the focus. Analysis of variance (ANOVA) was performed to compare the mean reconstructed shear modulus at different locations within each liver. The valid modulus reconstructions within $\pm 1 mm$ around the focus used to calculate the mean stiffness at each location were treated as independent measurements.

Stiffness and shear wave decorrelation rate measurements from all spatial locations interrogated in livers with the same pathological grading (e.g., fibrosis or steatosis scores) were combined to compare these measurements among the different groups. The mean of all the measured stiffness or decorrelation rate values was used to estimate the population mean of

each group. The 95% confidence interval for the population mean was calculated based on a two-stage nested sampling model (Mendenhall and Sincich, 1992). Sources of variation were partitioned into differences in the measured value of interest between different livers, and inhomogeneity within each liver.

Analysis of liver stiffness and quantitative measurements of fibrosis were performed by calculating the mean stiffness of each liver over all spatial locations interrogated. A linear regression model and the method of least squares was used to fit the mean stiffness of each liver to quantitative measures of fibrosis. The coefficient of determination (r^2) and p-value are reported for the linear fits. The same analysis was also performed for the measured shear wave decorrelation.

Results

Typical regression window lengths used for shear wave speed estimation were approximately 5*mm*, and resulted in overlapping windows in adjacent push locations. For each individual rat liver, the total number of locations with valid stiffness reconstructions ranged from 31 to 135 throughout the entire liver. The number of reconstructions obtained for healthy livers was reduced due to their small size and position underneath the ribs which provided a limited acoustic window for ultrasound (the mean and standard deviation of the weight of control livers was 18.0 ± 0.8*g*, compared to 24.1 ± 2.1*g* for treatment livers).

The reconstructed shear moduli at all spatial locations interrogated in two livers are shown in Figure 3. The top images show the shear modulus as a grayscale image overlaid on top of the reconstructed ultrasound coronal image (C-scan) at the same location. The C-scan image was formed by stacking the individual B-mode images acquired in each imaging plane (elevation dimension), and slicing through the 3D volume at the focal depth (25*mm*). The bottom images in Figure 3 show the modulus distribution for the same livers as a surface plot. It can be seen that the measured stiffness in these two livers are non-uniform. The shear modulus of Rat 6 increases in the elevation direction, while the shear modulus of Rat 8 peaked in the lateral dimension.

ANOVA showed that statistically significant differences ($p < 0.05$) in mean shear moduli at different spatial locations existed for all the livers imaged. In general, the spatial distribution of stiffness did not show an obvious pattern. In the liver of Rat 6, the distance from the focal depth of each excitation location to the liver edge was manually estimated from B-mode ultrasound images. There was no significant linear correlation between the shear modulus and location from the edge of the liver ($P = 0.1$). The mean shear moduli of each liver over all spatial locations interrogated is summarized in Figure 4. It can be seen that spatial variability (*i.e.* size of whiskers) in liver stiffness tends to increase with the mean shear modulus.

Histopathology results for the left and right liver lobes were very consistent. All five control animals had no fibrosis (F0), while all of the treatment animals had fibrotic livers, with six being staged as F3, and two livers each in F1 and F2 stages. The mean reconstructed shear moduli in all livers with the same fibrosis stage are shown in Figure 6(a). Due to the small number of animals with F1 and F2 livers, the confidence interval for the mean stiffness of these groups were considerably larger. The stiffness of all shear wave measurements in F0 livers was 1.5 ± 0.1*kPa* (*mean*±*CI*), compared to 1.8 ± 0.2*kPa* in F3 livers. The control animals all had low steatosis scores (≤ S1), while some treatment livers developed significant fatty change. The reconstructed shear moduli in livers with low (S0-S1) and high (S2-S3) steatosis scores are shown in Figure 6(b). The overlap of the confidence intervals indicate that differences in stiffness of the two groups were not statistically significant. Inflammation and hepatocyte

ballooning was minimal in all the rat livers. Only one liver had a NAS score above 4, which is diagnostic of NASH. This liver had a mean stiffness of 1.5*kPa* and a fibrosis score of F1.

Figure 8 shows typical slides stained with picosirius red for collagen quantification associated with the different fibrosis stages. Hepatocytes are stained green, while collagen is red. The mean and standard deviation of the measured stiffness within each liver are plotted against their percent fibrosis (percentage of the red pixels in sampled areas) in Figure 9. The linear regression between mean stiffness and percent fibrosis gave $r^2 = 0.43$, $p = 0.008$, and between stiffness inhomogeneity and percent fibrosis yielded $r^2 = 0.58$, $p = 0.001$. The hydroxyproline content of the rat livers are similarly shown in Figure 10 along with the mean and standard deviation of their measured stiffness. The results of linear regression between hydroxyproline and mean stiffness was $r^2 = 0.26$, $p = 0.054$, and between hydroxyproline and stiffness inhomogeneity was $r^2 = 0.48$, $p = 0.004$. The shear wave decorrelation rates observed in all spatial locations interrogated in each liver are summarized in Figure 5. Only one valid estimate was available for Rat 1 due to excessively noisy data. The decorrelation rates for the elastic phantom and FEM simulation are shown in the same figure as dotted lines. The overall decorrelation rates for livers at the various stages of fibrosis and steatosis are shown in Figure 7. Linear correlation between the mean decorrelation rate of each liver and fibrosis as quantified by picosirius red and hydroxyproline was not significant ($r^2 = 0.00$, $p = 0.96$ and $r^2 = 0.18$, $p = 0.12$, respectively).

No evidence of tissue damage from cavitation was observed in histological analysis of tissue slides. Stiffness measurements on rats with acoustic radiation force were performed non-invasively, and relatively quickly (total set-up and imaging time < 1*hr*), facilitating its possible use in future survival studies.

Discussion

The mean stiffness of rat livers increased with fibrosis stage. From the limited number of livers imaged, the F0 and F3 populations had non-overlapping 95% confidence intervals. This is consistent with other animal studies by Salameh et al (2007) and Yin et al (2007b), both of whom reported significant differences in MRE measured liver stiffness between healthy and fibrotic livers.

It is important to note that histological fibrosis grading is not a quantitative measure of the amount of fibrosis in the liver. As shown in Figure 8, the amount of fibrosis in the F2 liver and its measured stiffness is higher than the F3 liver. Indeed, distinctions between fibrosis grade are based primarily on the morphology of the fibrotic tissue, rather than the actual amount of fibrosis present in the liver (Kleiner et al, 2005). For example, the distinguishing feature of stage F3 is bridging between portal tracts. It is therefore not surprising that considerable variation in liver stiffness among patients with the same fibrosis stage have been observed in human studies (Rouvière et al, 2006;Huwart et al, 2006;Sandrin et al, 2003).

Picosirius red staining and hydroxyproline content, in contrast, are quantitative methods for evaluating the amount of collagen present in the liver (Jimenez et al, 1985; Reddy and Enwemeka, 1996). In this study, the collagen content of the liver determined by picosirius red staining and hydroxyproline assay were found to have a linear correlation with mean liver stiffness of $r^2 = 0.43$, $p = 0.008$ and $r^2 = 0.26$, $p = 0.054$, respectively. This suggests that changes in liver stiffness may be reflective of the collagen content within the liver. Using MRE and the same CCl_4 animal model, Salameh et al (2007) reported correlations of $r^2 = 0.49$, $p = 0.005$ between liver stiffness and fibrosis content measured using picosirius red, and $r^2 = 0.36$, $p = 0.016$ between stiffness and hydroxyproline content. The authors attributed the weaker correlation from hydroxyproline to the different liver locations where MR elastography and

hydroxyproline analysis were performed. The sample locations used for hydroxyproline assay in this study are also unlikely to correspond to the exact location where stiffness measurements are performed. Inter-sample variation in hydroxyproline analysis can be significant in livers where the distribution of fibrous tissue is heterogeneous (Gomes et al, 2006).

In contrast to liver biopsies where analysis is limited to a single core sample, acoustic radiation force can be used to measure stiffness at multiple points inside the liver non-invasively. By varying the excitation location and focal point, stiffness images showing the spatial distribution of shear modulus can be constructed, as shown in Figure 3. Therefore, acoustic radiation force has the potential to provide additional information about the spatial distribution of liver stiffness, which may also be diagnostically relevant.

Large variations of stiffness was observed in individual rat livers in the present study. The pattern of stiffness distribution varied between livers, with no consistent trends spatially. This behavior suggests that the observed inhomogeneities were not due to any underlying systematic measurement bias. The range of stiffness values measured within individual livers tended to increase with mean stiffness (see Figure 4). Palmeri et al (2008) has previously shown that the variance of shear moduli reconstructed with the Lateral TTP algorithm increases with stiffness of the medium interrogated. However, due to the small range in liver stiffness encountered in this study, the impact of this source of additional variation on the reconstructed shear moduli herein is minimal.

The linear correlation between the standard deviation in stiffness of each liver with percent fibrosis and liver hydroxyproline content were $r^2 = 0.58$, $p = 0.001$, and $r^2 = 0.48$, $p = 0.004$, respectively. This suggests that stiffness inhomogeneity increased with fibrosis in the rat livers. These results are consistent with those obtained by Salameh et al (2007) and Huwart et al (2006) using MRE. Huwart et al (2006) reported increasing heterogeneity in measured stiffness and viscosity maps in patient livers with higher grades of fibrosis. Likewise, Salameh et al (2007) observed linear correlations between the standard deviation of measured viscoelastic properties with percent fibrosis induced in rat livers using the CCL_4 model.

Increase in stiffness heterogeneity could serve as an additional measure of liver fibrosis. However, this also means that the liver must be adequately sampled spatially to fully characterize its stiffness. In the present study, a relatively small number of valid modulus reconstructions were obtained for the control livers, due to their smaller size compared to the treated livers and the limited acoustic window available. Therefore, the mean stiffness of the control livers are subject to greater uncertainty from under-sampling. On the other hand, this effect may be mitigated by the more homogeneous distribution of stiffness in healthy livers.

The recent work of Georges et al (2007) suggest that increased liver stiffness may be linked to the development of early fibrosis. Using the CCL_4 model on rats and a strain rheometer to measure the shear storage modulus in *ex vivo* samples, Georges et al (2007) did not observe statistically significant correlations between measured liver stiffness and fibrosis (quantified by picosirius red staining as well as histology). Instead, significant increases in liver stiffness before the presence of fibrosis in the liver at early time points (3 – 10 days after the start of treatment) were detected. After 28 days, Georges et al (2007) reported only marginal increases in the liver stiffness compared to earlier time points, while the amount of fibrosis grew substantially. In contrast, the present study detected a significant ($p = 0.008$) linear correlation between liver stiffness and percent fibrosis measured by picosirius red. This inconsistency could be attributed to many causes. Firstly, the study herein examined livers only at a later time point in the model, when a linear relationship between fibrosis and stiffness may exist. In addition, liver stiffness was measured by Georges et al (2007) in excised *ex vivo* samples, while stiffness measurements were conducted *in vivo* in the present study. Nevertheless, the results

of Georges et al (2007) suggest that increased liver stiffness may precede the early stages of fibrosis. Thus, a noninvasive method for measuring liver stiffness, such as acoustic radiation force, could play an important role in the study of fibrogenesis and may be potentially used to identify individuals at high risk of developing liver fibrosis.

Other factors, besides collagen content, may also influence liver stiffness. In particular, the degree of steatosis was found to be appreciable for the CCl_4 treated livers. One might expect the presence of fat to soften the liver, thus lowering the shear modulus of the fibrotic livers. In a recent study with MR elastography, Yin et al (2007b) found no significant correlation between liver stiffness and fat content, but significant correlation between stiffness and the amount of fibrosis in a genetically induced mouse model of liver fibrosis. The authors suggested that liver stiffness is dominated by the presence of fibrosis, and unaffected by the amount of fat. In our study, no significant change in mean stiffness measured in livers with low fat content (S0–S1) and high fat content (S2–S3) was observed, consistent with the findings of Yin et al (2007b). The effect of fat content on liver stiffness could be further explored using models of liver disease in which either fibrosis or fat infiltration occur independently (Koteish and Diehl, 2001).

The lateral TTP algorithm used for shear modulus reconstruction in the present study estimates the speed at which the peak shear wave displacement amplitude travels. In a dispersive medium, this time-of-flight method will measure the shear wave 'bulk' velocity, which lies in-between the speeds of its fastest and slowest frequency components. It can be seen from Figure 5 that shear waves propagating in the rat livers are subject to greater loss in spatial coherence compared to an elastic phantom and elastic FEM simulation. This suggests that dispersive spreading of the shear wave wavepacket from the viscoelastic nature of the liver tissue was occurring during propagation. Although there was no relationship between fibrosis and shear wave decorrelation rates evaluated herein, the studies of Salameh et al (2007) suggest that fibrosis leads to an increase in liver shear viscosity. Thus, further work in quantification of viscoelastic parameters of the liver with our data and investigating their relationship with liver fibrosis is being currently being pursued.

No experimental model of liver fibrosis reproduces the exact etiology of human disease. The CCl_4 rat model in this study produced a change of only $0.4kPa$ in mean measured stiffness of healthy (F0) and fibrotic (F3) livers, consistent with the small range in mean stiffness observed by Salameh et al (2007) between normal and fibrotic rat livers ($1.76 – 2.29kPa$) using the same model and MR elastography. However, much larger stiffness values in human livers with fibrosis have been reported. Rouvière et al (2006) measured the mean liver stiffness among 11 patients with various stages of fibrosis to be $5.6kPa$ (range $2.7 – 19.2kPa$), compared to a mean of $2.0kPa$ for healthy volunteers using MR elastography. Sandrin et al (2003) reported a very large range in stiffness in patients with cirrhosis ($4.7 – 23kPa$) with the Fibroscan® device. In preliminary human studies in our laboratory using the radiation force techniques outlined herein, stiffness ranges between $1 – 3kPa$ have been observed for livers with fibrosis stages between F0 and F3. It is unlikely that the full spectrum of characteristics of human disease can be emulated using one animal model alone. Therefore, the use of other models which more closely resemble a specific human liver disease could be explored in the future.

Conclusion

This study has demonstrated the feasibility of acoustic radiation force as a non-invasive method for the quantitative assessment of liver fibrosis in small animals. The mean stiffness of fibrotic (F3) rat livers, as measured by acoustic radiation force, was $1.8 \pm 0.2kPa$ (*mean*±*CI*), compared with $1.5 \pm 0.1kPa$ for healthy livers, with non-overlapping 95% confidence intervals. Liver stiffness measured by acoustic radiation force was linearly correlated with the amount of

fibrosis in the liver as quantitatively measured by picosirius red staining ($r^2 = 0.43$, $p = 0.008$). Therefore, liver stiffness may be reflective of the collagen content of the liver. In addition, the spatial heterogeneity of liver stiffness was also found to have a significant positive linear relationship with the amount of fibrosis ($r^2 = 0.58$, $p = 0.001$). These results suggest that acoustic radiation force stiffness estimation methods can provide a quantitative evaluation of the extent of fibrosis in the liver and may be useful in the diagnosis, management, and study of liver fibrosis.

Acknowledgments

This work was supported by NIH grant 2R01 EB-002132. The authors would like to thank Center for In Vivo Microscopy staff, Ned Rouze, and Liang Zhai for help in animal experiments, and Siemens Medical Solutions, USA, for their system support.

References

Arena U, Vizzutti F, Corti G, Ambu S, Stasi C, Bresci S, Moscarella S, Boddi V, Petrarca A, Laffi G, Marra F, Pinzani M. Acute viral hepatitis increases liver stiffness values measured by transient elastography. Hepatology 2008;47(2):380–384. [PubMed: 18095306]

Ashfaq, M.; Huttebrauker, N.; Hansen, C.; Wilkening, W.; Ermert, H. Spatial compounding with tissue harmonic images and monostatic synthetic aperture reconstruction; Proceedings of the 2005 IEEE Ultrasonics Symposium; Rotterdam, The Netherlands. September 2005; p. 1220-1223.

Bercoff J, Tanter M, Fink M. Supersonic shear imaging: a new technique for soft tissue elasticity mapping. IEEE Trans Ultrason Ferroelectr Freq Control 2004;51(4):396–409. [PubMed: 15139541]

Carrión JA, Navasa M, Bosch J, Bruguera M, Gilabert R, Forns X. Transient elastography for diagnosis of advanced fibrosis and portal hypertension in patients with hepatitis C recurrence after liver transplantation. Liver Transpl 2006;12(12):1791–1798. [PubMed: 16823833]

Castéra L, Vergniol J, Foucher J, Le Bail B, Chanteloup E, Haaser M, Darriet M, Couzigou P, De Lédinghen V. Prospective comparison of transient elastography, fibrotest, apri, and liver biopsy for the assessment of fibrosis in chronic hepatitis C. Gastroenterology 2005;128(2):343–350. [PubMed: 15685546]

Chen S, Fatemi M, Greenleaf JF. Quantifying elasticity and viscosity from measurement of shear wave speed dispersion. J Acoust Soc Am 2004;115(6):2781–2785. [PubMed: 15237800]

Fahey BJ, Nightingale KN, Nelson RC, Palmeri ML, Trahey GE. Acoustic radiation force impulse imaging of the abdomen: demonstration of feasibility and utility. Ultrasound Med Biol 2005;31(9): 1185–1198. [PubMed: 16176786]

Foucher J, Castéra L, Bernard PH, Adhoute X, Laharie D, Bertet J, Couzigou P, de Lédinghen V. Prevalence and factors associated with failure of liver stiffness measurement using fibroscan in a prospective study of 2114 examinations. Eur J Gastroen Hepat 2006;18(4):411–412.

Friedman SL. Liver fibrosis - from bench to bedside. J Hepatol 2003;38:S38–S53. [PubMed: 12591185]

Fry WJ, Fry RB. Temperature changes produced in tissue during ultrasonic irradiation. J Acoust Soc Am 1953;25(1):6–11.

Georges PC, Hui JJ, Combos Z, McCormick ME, Wang AY, Uemura M, Mick R, Janmey PA, Furth EE, Wells RG. Increased stiffness of the rat liver precedes matrix deposition: implications for fibrosis. Am J Physiol Gastrointest Liver Physiol 2007;293(6):G1147–G1154. [PubMed: 17932231]

Gomes ATB, Bastos CG, Afonso CL, Medrado BF, Andrade ZA. How variable are hydroxyproline determinations made in different samples of the same liver? Clin Biochem 2006;39(12):1160–1163. [PubMed: 17005170]

Huwart L, Peeters F, Sinkus R, Annet L, Salameh N, ter Beek LC, Horsmans Y, Van Beers BE. Liver fibrosis: non-invasive assessment with MR elastography. NMR Biomed 2006;19:173–179. [PubMed: 16521091]

Jimenez W, Parés A, Caballría J, Heredia D, Bruguera M, Torres M, Rojkind M, Rodés J. Measurement of fibrosis in needle liver biopsies: evaluation of a colorimetric method. Hepatology 1985;5(5):815–818. [PubMed: 4029893]

Kleiner DE, Brunt EM, Natta MV, Behling C, Contos MJ, Cummings OW, Ferrell LD, Liu YC, Torbenson MS, Unalp-Arida A, Yeh M, McCullough AJ, Sanyal AJ. Design and validation of a histological scoring system for nonalcoholic fatty liver disease. Hepatology 2005;41(6):1313–1321. [PubMed: 15915461]

Konofagou EE, Hynynen K. Localized harmonic motion imaging: Theory, simulations and experiments. Ultrasound Med Biol 2003;29(10):1405–1413. [PubMed: 14597337]

Koteish A, Diehl AM. Animal models of steatosis. Semin Liver Dis 2001;21(1):89–104. [PubMed: 11296700]

McAleavey SA, Menon M, Orszulak J. Shear-modulus estimation by application of spatially modulated impulsive acoustic radiation force. Ultrasonic Imaging 2007;29(2):87–104. [PubMed: 17679324]

McDannold N, Maier S. Magnetic resonance acoustic radiation force imaging. Med Phys 2008;35(8): 3748–3758. [PubMed: 18777934]

Mendenhall, W.; Sincich, T. Statistics for Engineering and the Sciences. Vol. 3. Macmillan; New York: 1992.

Nightingale K, Soo MS, Nightingale R, Trahey G. Acoustic radiation force impulse imaging: in vivo demonstration of clinical feasibility. Ultrasound Med Biol 2002;28(2):227–235. [PubMed: 11937286]

Nyborg, WL. Acoustic streaming. In: Mason, W., editor. Physical Acoustics. Vol. IIB. Academic Press; New York: 1965. p. 265-331.

Nyborg WL. Heat generation by ultrasound in a relaxing medium. J Acoust Soc Am 1981;70(2):310–312.

Palmeri ML, Sharma AC, Bouchard RR, Nightingale RW, Nightingale KR. A finite-element method model of soft tissue response to impulsive acoustic radiation force. IEEE Trans Ultrason Ferroelectr Freq Control 2005;52(10):1699–1712. [PubMed: 16382621]

Palmeri ML, Wang MH, Dahl JJ, Frinkley KD, Nightingale KR. Quantifying hepatic shear modulus in vivo using acoustic radiation force. Ultrasound Med Biol 2008;34(4):546–558. [PubMed: 18222031]

Piccinino F, Sagnelli E, Pasquale G, Giusti G. Complications following percutaneous liver biopsy, a multicentre retrospective study on 68,276 biopsies. J Hepatol 1986;2(2):165–173. [PubMed: 3958472]

Pinton GF, Dahl JJ, Trahey GE. Rapid tracking of small displacements with ultrasound. IEEE Trans Ultrason Ferroelectr Freq Control 2006;53(6):1103–1117. [PubMed: 16846143]

Ratziu V, Charlotte F, Heurtier A, Gombert S, Giral P, Bruckert E, Grimaldi A, Capron F, Poynard T. Sampling variability of liver biopsy in nonalcoholic fatty liver disease. Gastroenterology 2005;128 (7):1898–1906. [PubMed: 15940625]

Reddy GK, Enwemeka CS. A simplified method for the analysis of hydroxyproline in biological tissues. Clin Biochem 1996;29(3):225–229. [PubMed: 8740508]

Rouvière O, Yin M, Dresner MA, Rossman PJ, Burgart LJ, Fidler JL, Ehman RL. MR elastography of the liver: Preliminary results. Radiology 2006;240(2):440–448. [PubMed: 16864671]

Salameh N, Peeters F, Sinkus R, Abarca-Quinones J, Annet L, Ter Beek LC, Leclercq I, Van Beers BE. Hepatic viscoelastic parameters measured with MR elastography: Correlations with quantitative analysis of liver fibrosis in the rat. J Magn Reson Imaging 2007;26(4):956–962. [PubMed: 17896384]

Sandrin L, Fourquet B, Hasquenoph JM, Yon S, Fournier C, Mai F, Christidis C, Ziol M, Poulet B, Kazemi F, Beaugrand M, Palau R. Transient elastography: a new noninvasive method for assessment of hepatic fibrosis. Ultrasound Med Biol 2003;29(12):1705–1713. [PubMed: 14698338]

Sarvazyan AP, Rudenko OV, Swanson SD, Fowlkes JB, Emelianov SY. Shear wave elasticity imaging: a new ultrasonic technology of medical diagnostics. Ultrasound Med Biol 1998;24(9):1419–1435. [PubMed: 10385964]

Takeda T, Yasuda T, Nakayama Y, Nakaya M, Kimura M, Yamashita M, Sawada A, Abo K, Takeda S, Sakaguchi H, Shiomi S, Asai H, Seki S. Usefulness of noninvasive transient elastography for assessment of liver fibrosis stage in chronic hepatitis C. World J Gastroenterol 2006;12(48):7768–7773. [PubMed: 17203518]

Tanter M, Bercoff J, Athanasiou A, Deffieux T, Gennisson JL, Montaldo G, Muller M, Tardivon A, Fink M. Quantitative assessment of breast lesion viscoelasticity: initial clinical results using supersonic shear imaging. Ultrasound Med Biol 2008;34(9):1373–1386. [PubMed: 18395961]

Teotico GA, Miller RJ, Frizzell LA, Zachary JF, O'Brien WD Jr. Attenuation coefficient estimates of mouse and rat chest wall. IEEE Trans Ultrason Ferroelectr Freq Control 2001;48(2):593–601. [PubMed: 11370373]

Tsukamoto H, Matsuoka M, French SW. Experimental models of hepatic fibrosis: a review. Semin Liver Dis 1990;10(1):56–65. [PubMed: 2110685]

Yamaguchi K, Yang L, McCall S, Huang J, Yu XX, Pandey SK, Bhanot S, Monia BP, Li YX, Diehl AM. Inhibiting triglyceride synthesis improves hepatic steatosis but exacerbates liver damage and fibrosis in obese mice with nonalcoholic steatohepatitis. Hepatology 2007;45(6):1366–1374. [PubMed: 17476695]

Yeh WC, Li PC, Jeng YM, Hsu HC, Kuo PL, Li ML, Yang PM, Lee PH. Elastic modulus measurements of human liver and correlation with pathology. Ultrasound Med Biol 2002;28(4):467–474. [PubMed: 12049960]

Yin M, Talwalkar JA, Glaser KJ, Manduca A, Grimm RC, Rossman PJ, Fidler JL, Ehman RL. Assessment of hepatic fibrosis with magnetic resonance elastography. Clin Gastroenterol Hepatol 2007a;5(10):1207–1213. [PubMed: 17916548]

Yin M, Woollard J, Wang X, Torres VE, Harris PC, Ward CJ, Glaser KJ, Manduca A, Ehman RL. Quantitative assessment of hepatic fibrosis in an animal model with magnetic resonance elastography. Magn Reson Med 2007b;58(2):346–353. [PubMed: 17654577]

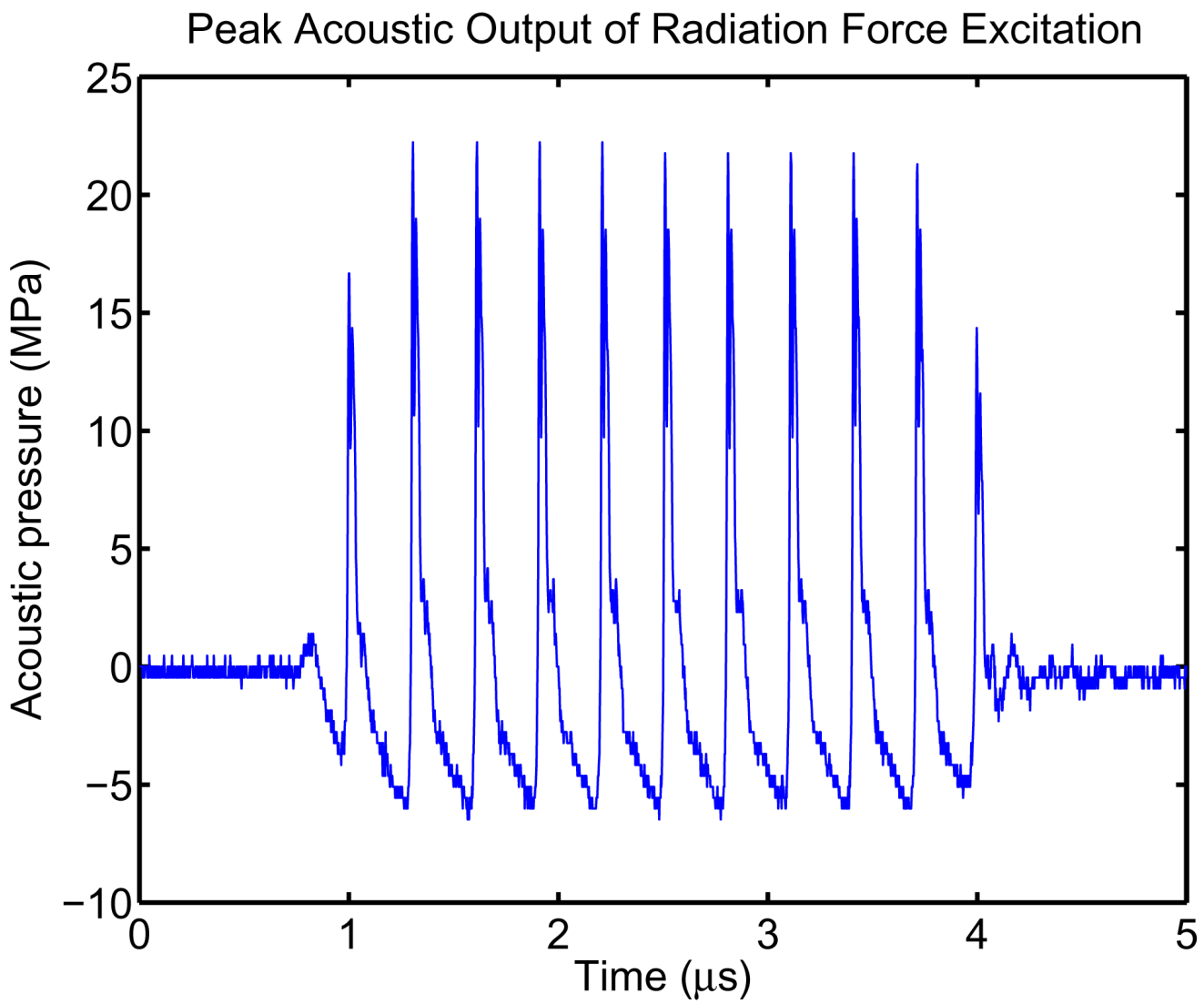

Figure 1.
Peak pressure of the radiation force excitation field measured with a hydrophone. The amplitude has been scaled by derating factors accounting for the acoustic attenuation of the rat abdominal wall, rat liver, and power supply droop over 200 cycles of the pushing pulse.

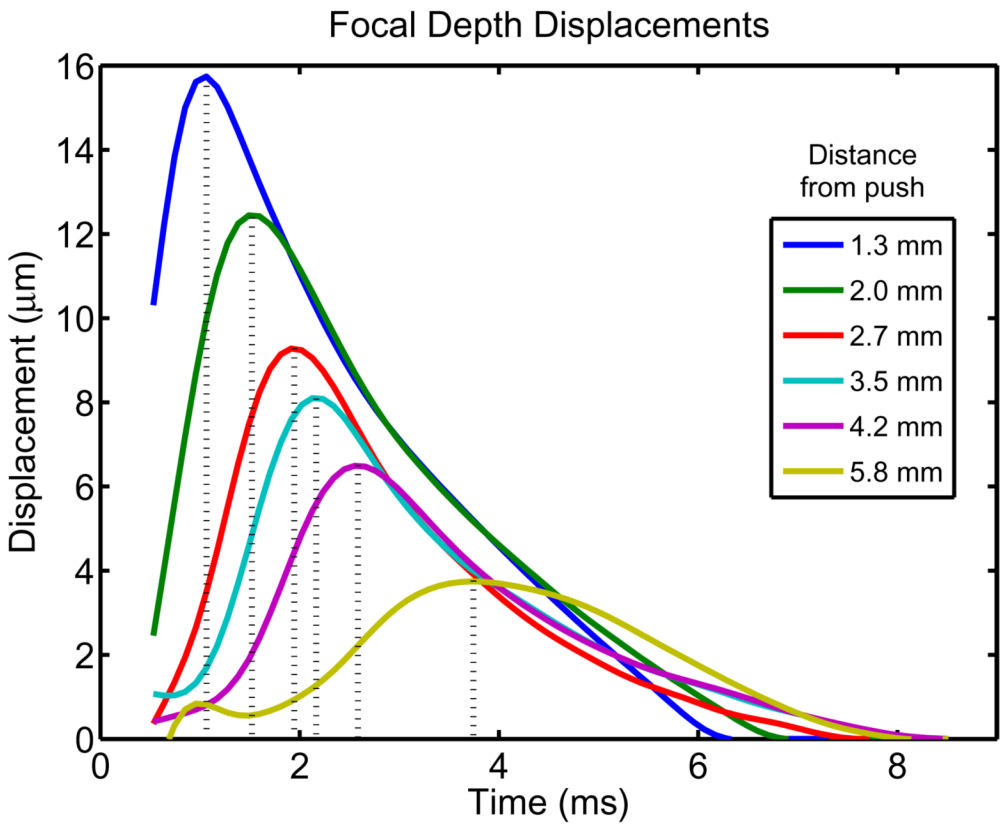

Figure 2.
Tissue axial displacement at the focal depth measured *in vivo* in one rat liver after radiation force excitation. Each curve shows the tissue displacement as a function of time after the excitation. The lateral location of each curve with respect to the excitation location are shown in the legend. The vertical dotted lines show the measured TTP values used for shear wave speed estimation. The back edge of the displacement curve is tied to zero beyond the maximum expected transit time of the shear wave by the dynamic motion filter.

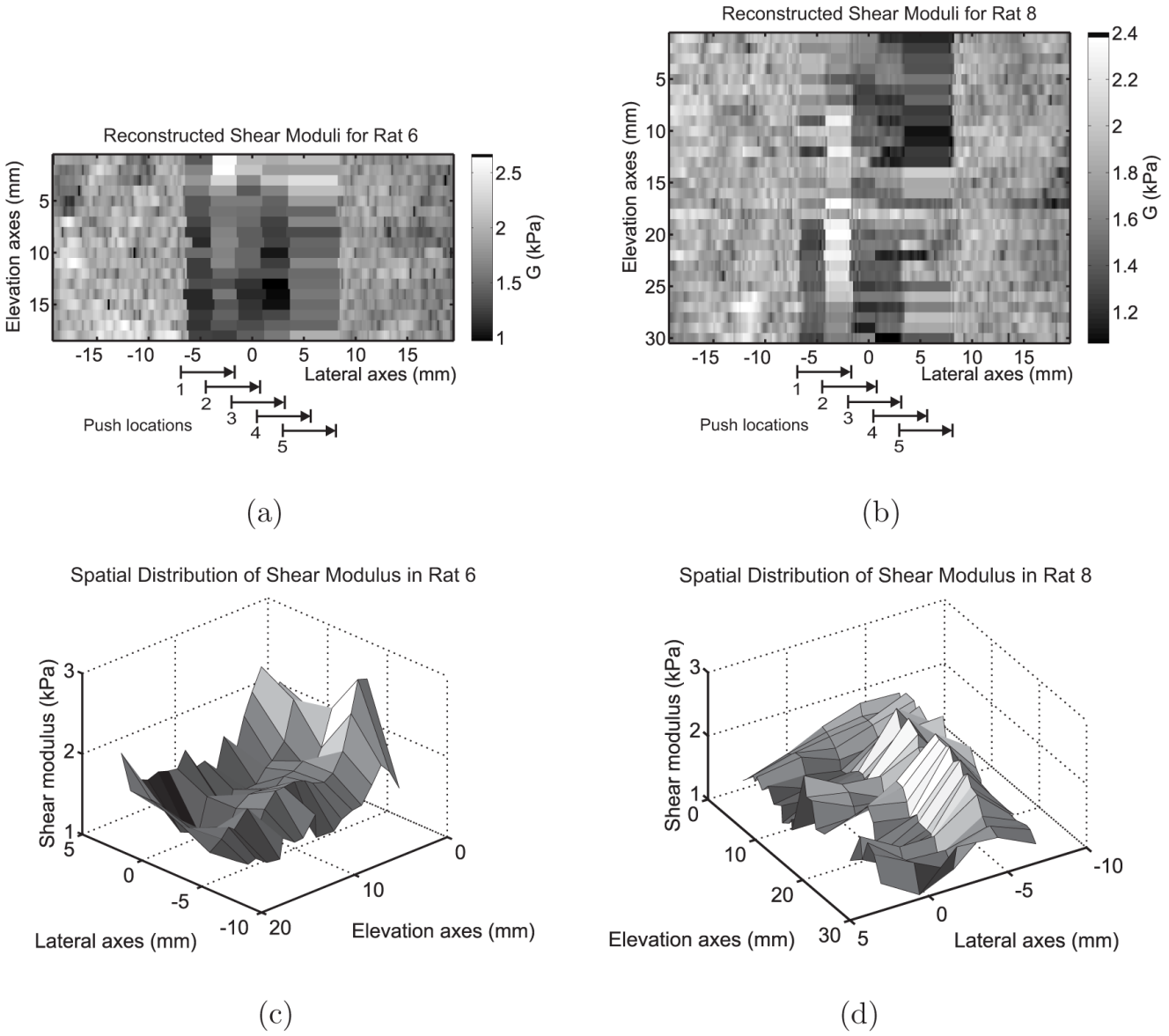

Figure 3.

Reconstructed shear modulus at all spatial locations for two livers. The shear modulus is shown as an image overlaid on top of the reconstructed ultrasound C-scan at the same location (top row). The shear modulus is displayed as a surface plot (bottom row).

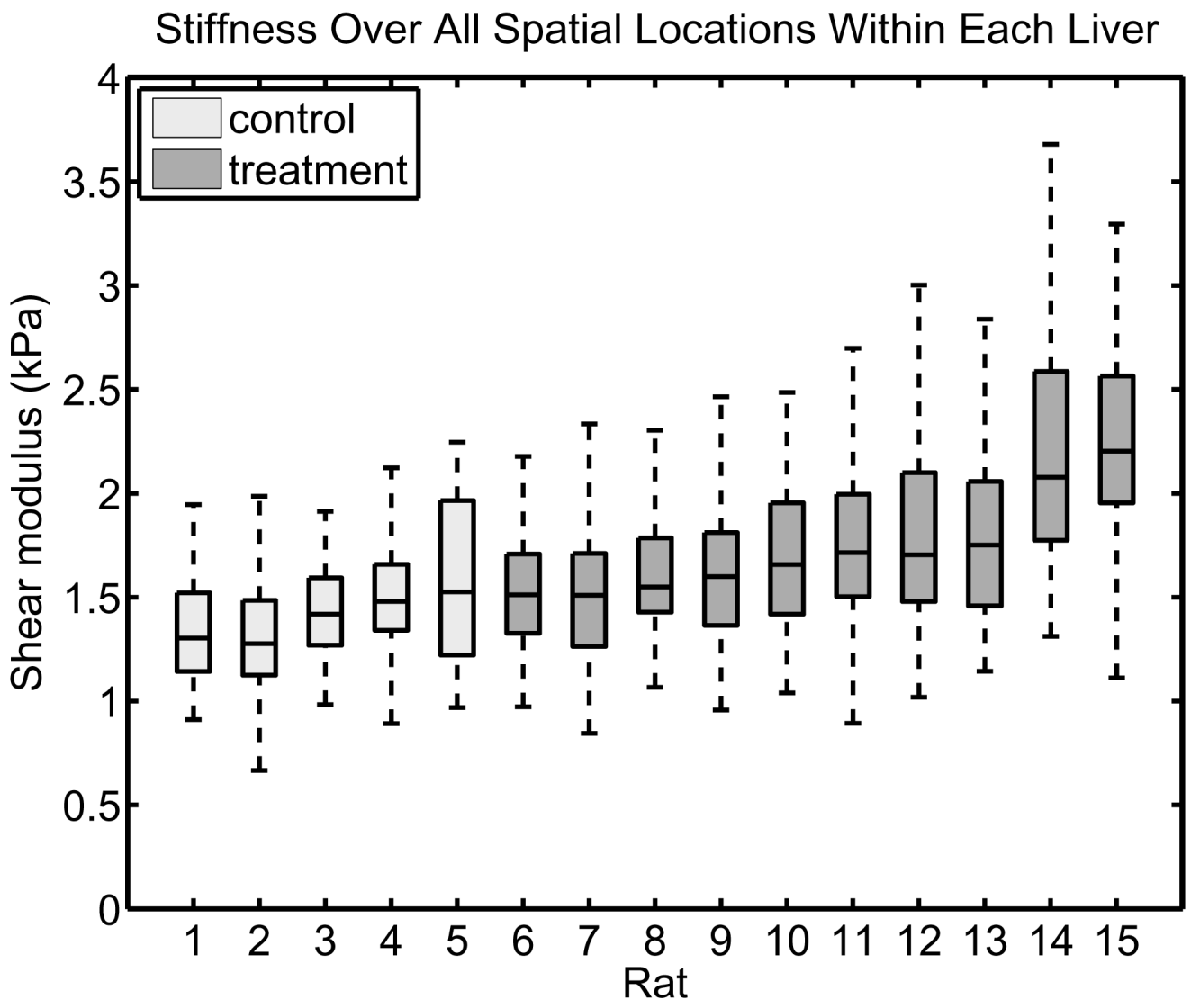

Figure 4.
Boxplot of reconstructed shear modulus for all spatial locations interrogated in the 15 livers. Outliers beyond 1.5× the interquartile range have been omitted.

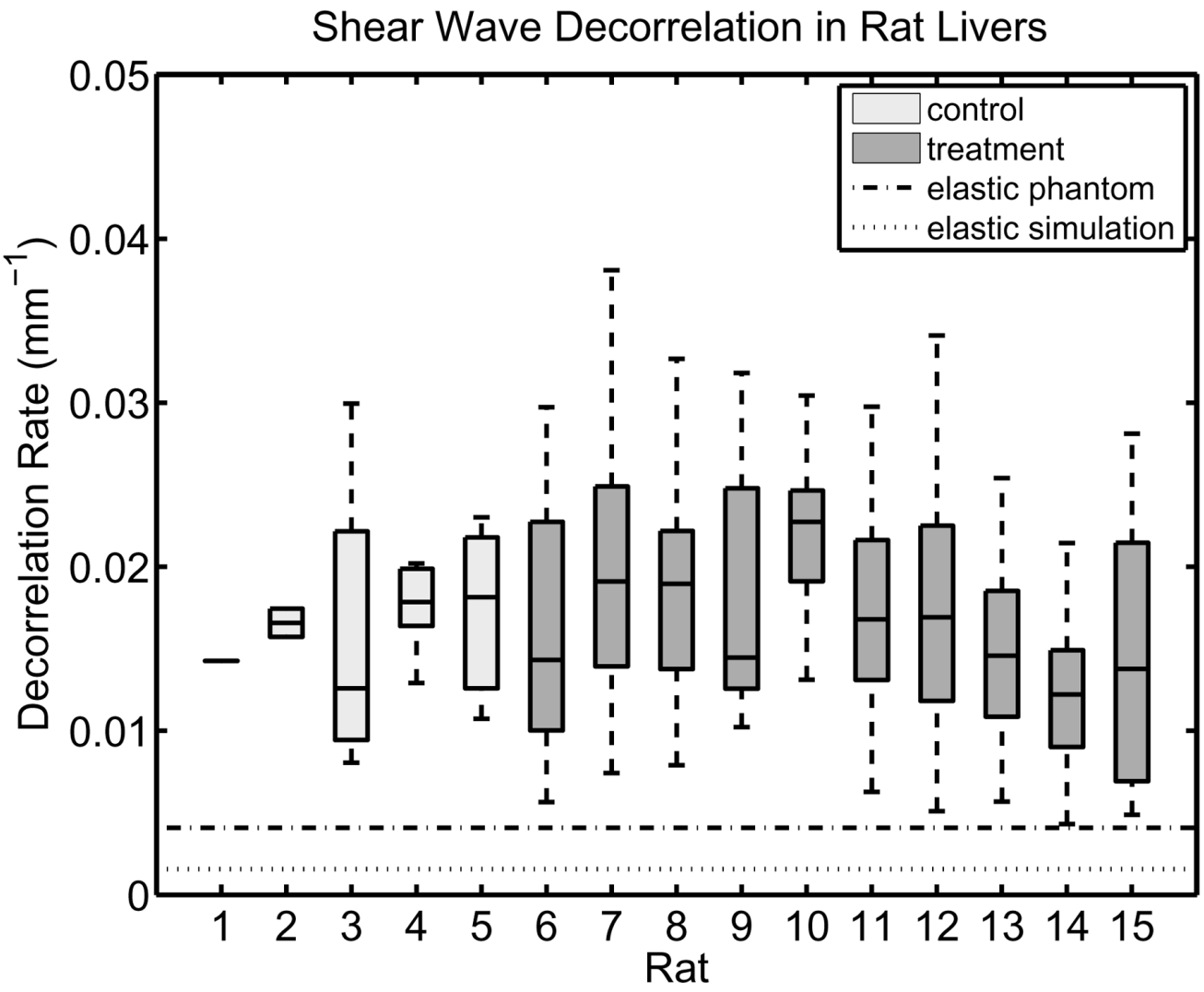

Figure 5.
Boxplot of shear wave decorrelation rates at all spatial locations interrogated in each liver. Results are also shown for simulated data in a purely elastic medium and propagation in a purely elastic phantom for comparison.

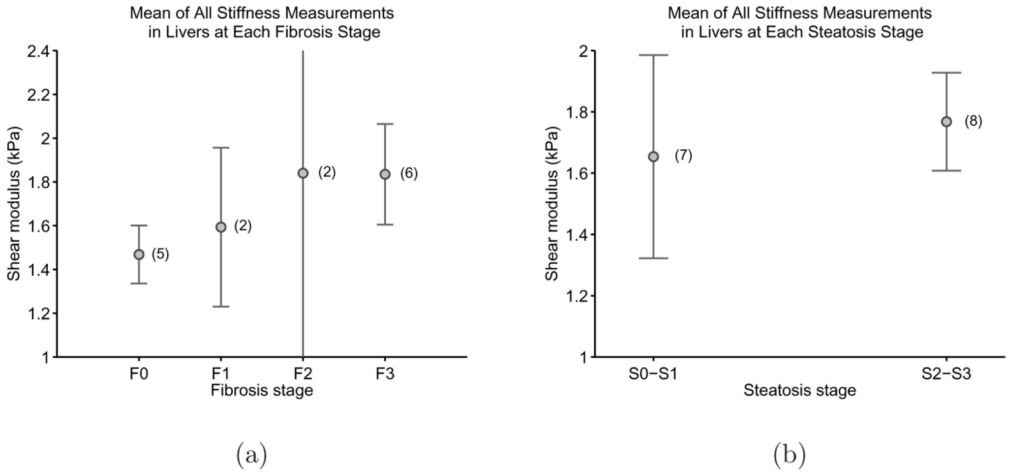

Figure 6.

Mean stiffness of all shear wave measurements in livers with the same fibrosis stage 6(a), and in livers with low (S0–S1) and high (S2–S3) steatosis scores 6(b). The 95% CI for the mean is shown as error bars. The CI for F2 rats was ±4.2*kPa*. The The number of livers from which stiffness measurements were averaged in each group is shown in parentheses.

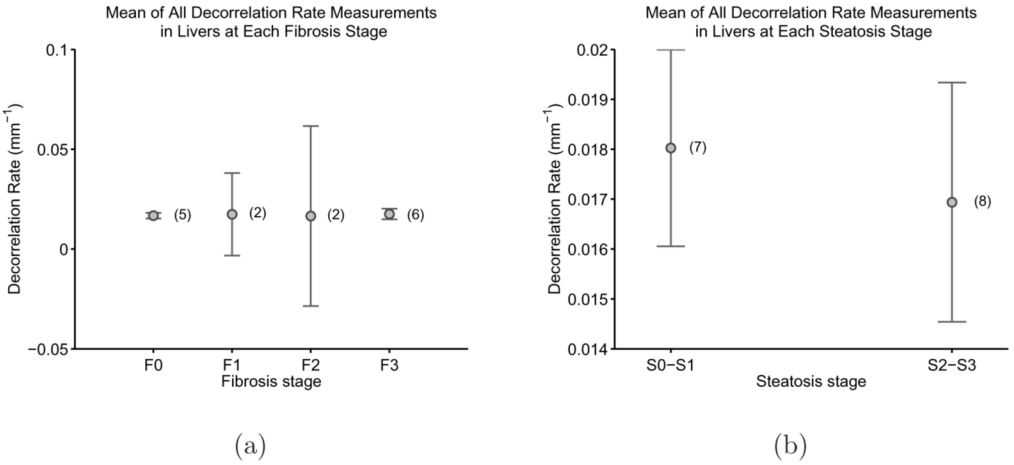

Figure 7.

Mean decorrelation rate of all shear wave measurements in livers with the same fibrosis stage 7(a), and in livers with low (S0–S1) and high (S2–S3) steatosis scores 7(b). The 95% CI for the mean is shown as error bars. The The number of livers from which stiffness measurements were averaged in each group is shown in parentheses.

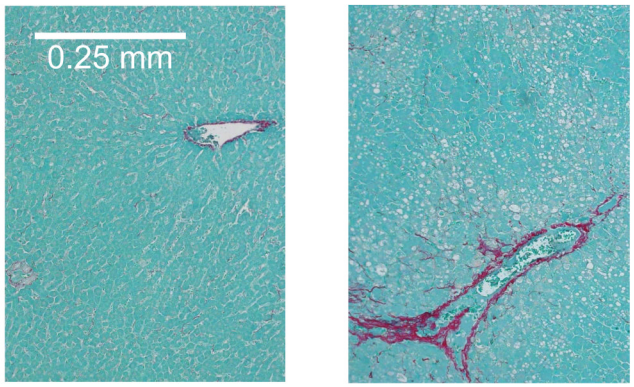

(a) F0 (1.0%) $G = 1.4 \pm 0.2kPa$

(b) F1 (3.3%) $G = 1.5 \pm 0.3kPa$

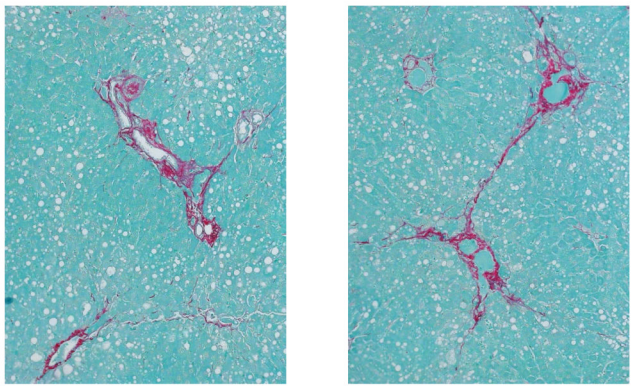

(c) F2 (13.1%) $G = 2.2 \pm 0.5kPa$

(d) F3 (10.3%) $G = 1.7 \pm 0.4kPa$

Figure 8.
Sections of 4 rat livers stained with picosirius red used for collagen quantification. The corresponding fibrosis score, percentage fibrosis, and measured stiffness is shown for each liver.

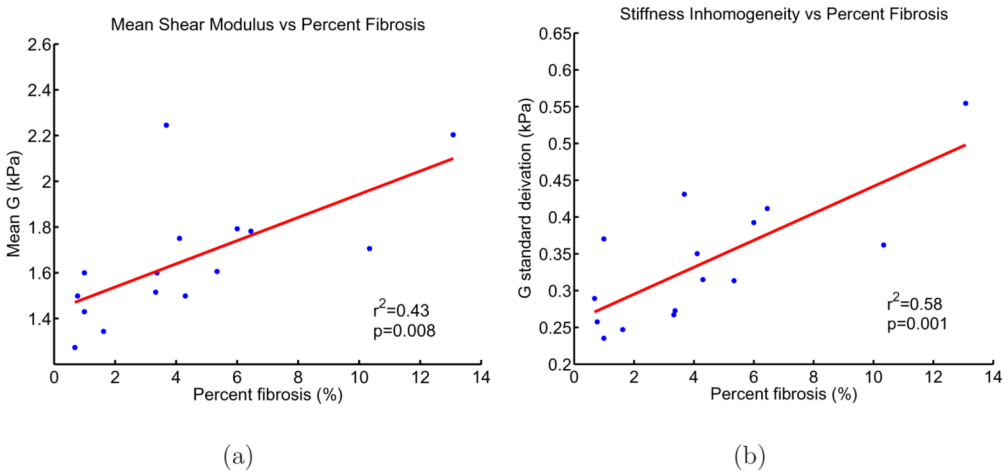

Figure 9.

Mean stiffness 9(a), and its standard deviation 9(b) over all spatial locations interrogated, as a function of percent fibrosis from picosirius red staining for all livers. The linear regression line, coefficient of determination, and p-value are shown in each case.

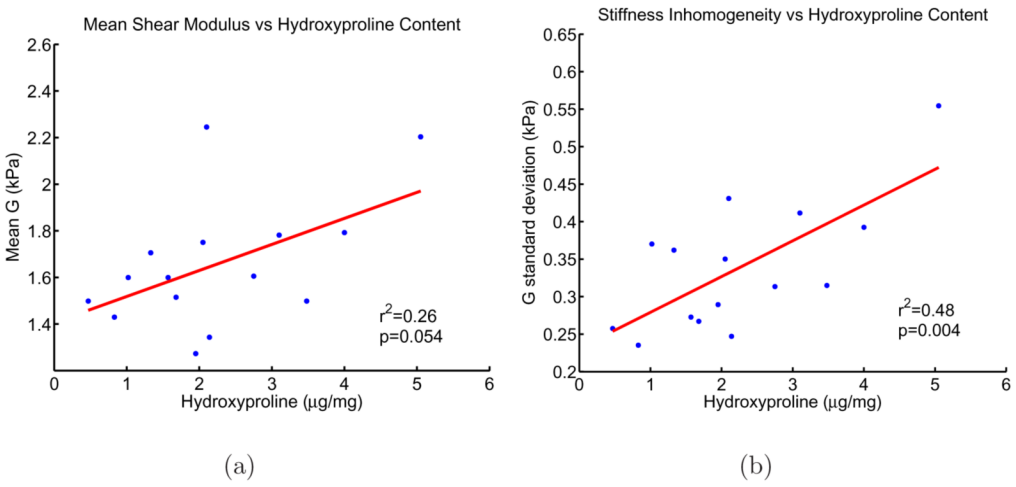

Figure 10.

Mean stiffness 10(a), and its standard deviation 10(b) over all spatial locations interrogated, as a function of hydroxyproline content for all livers. The linear regression line, coefficient of determination, and p-value are shown in each case.

Table 1

Summary of radiation force sequence parameters.

Parameter	Value
Probe	VF7-3
Push freq	3.3MHz
Track freq	7.27MHz
Push cycles	200
Push duration	61μs
PRF	9.4kHz
Push F#	2.0
Push focal depth (lateral)	25mm
Elevation focus	37.5mm
ΔT	0.18°C
I_{sppa}	$3054 W/cm^2$
MI (0.3)	3.98
MI (*in situ*)	3.6